Conference Proceedings of the Society for Experimental Mechanics Series

Gaetan Kerschen · Douglas Adams · Alex Carrella *Editors*

Topics in Nonlinear Dynamics, Volume 1

Proceedings of the 31st IMAC, A Conference on Structural Dynamics, 2013

SEM

Springer

Conference Proceedings of the Society for Experimental Mechanics Series

Series Editor

Tom Proulx
Society for Experimental Mechanics, Inc.,
Bethel, CT, USA

For further volumes:
http://www.springer.com/series/8922

Gaetan Kerschen • Douglas Adams • Alex Carrella
Editors

Topics in Nonlinear Dynamics, Volume 1

Proceedings of the 31st IMAC, A Conference on Structural Dynamics, 2013

Springer

Editors
Gaetan Kerschen
University of Liege
Liege, Belgium

Alex Carrella
LMS International
Brussels, Belgium

Douglas Adams
School of Mechanical Engineering
Purdue University
West Lafayette, USA

ISSN 2191-5644 ISSN 2191-5652 (electronic)
ISBN 978-1-4614-6569-0 ISBN 978-1-4614-6570-6 (eBook)
DOI 10.1007/978-1-4614-6570-6
Springer New York Heidelberg Dordrecht London

Library of Congress Control Number: 2013932475

© The Society for Experimental Mechanics, Inc. 2013
This work is subject to copyright. All rights are reserved by the Publisher, whether the whole or part of the material is concerned, specifically the rights of translation, reprinting, reuse of illustrations, recitation, broadcasting, reproduction on microfilms or in any other physical way, and transmission or information storage and retrieval, electronic adaptation, computer software, or by similar or dissimilar methodology now known or hereafter developed. Exempted from this legal reservation are brief excerpts in connection with reviews or scholarly analysis or material supplied specifically for the purpose of being entered and executed on a computer system, for exclusive use by the purchaser of the work. Duplication of this publication or parts thereof is permitted only under the provisions of the Copyright Law of the Publisher's location, in its current version, and permission for use must always be obtained from Springer. Permissions for use may be obtained through RightsLink at the Copyright Clearance Center. Violations are liable to prosecution under the respective Copyright Law.
The use of general descriptive names, registered names, trademarks, service marks, etc. in this publication does not imply, even in the absence of a specific statement, that such names are exempt from the relevant protective laws and regulations and therefore free for general use.
While the advice and information in this book are believed to be true and accurate at the date of publication, neither the authors nor the editors nor the publisher can accept any legal responsibility for any errors or omissions that may be made. The publisher makes no warranty, express or implied, with respect to the material contained herein.

Printed on acid-free paper

Springer is part of Springer Science+Business Media (www.springer.com)

Preface

Topics in Nonlinear Dynamics represents one of seven volumes of technical papers presented at the 31st IMAC, A Conference and Exposition on Structural Dynamics, 2013 organized by the Society for Experimental Mechanics, and held in Garden Grove, California February 11–14, 2013. The full proceedings also include volumes on Experimental Dynamics Substructuring; Dynamics of Bridges; Dynamics of Civil Structures; Model Validation and Uncertainty Quantification; Special Topics in Structural Dynamics; and, Modal Analysis.

Each collection presents early findings from experimental and computational investigations on an important area within Structural Dynamics. Nonlinearity is one of these areas.

The vast majority of real engineering structures behave nonlinearly. Therefore, it is necessary to include nonlinear effects in all the steps of the engineering design: in the experimental analysis tools (so that the nonlinear parameters can be correctly ***identified***) and in the mathematical and numerical models of the structure (in order to run accurate ***simulations***). In so doing, it will be possible to create a model representative of the reality which (once ***validated***) can be used for better predictions.

Several nonlinear sessions will address theoretical and numerical aspects of nonlinear dynamics (covering rigorous theoretical formulations and robust computational algorithms) as well as experimental techniques and analysis methods. There are papers dedicated to nonlinearity in practice where real-life examples of nonlinear structures will be discussed. Finally, a number of papers will discuss an interesting shift in paradigm: nonlinearities are not always detrimental, but instead they can be exploited for better engineering designs.

The organizers would like to thank the authors, presenters, session organizers, and session chairs for their participation in this track.

Liege, Belgium — Gaetan Kerschen
West Lafayette, USA — Douglas Adams
Brussels, Belgium — Alex Carrella

Contents

Chapter 1
International Space Station 2A Array Modal Analysis

Michael Laible, Kristin Fitzpatrick, and Michael Grygier

Abstract On December 9th 2009, the International Space Station (ISS) 2A solar array mast experienced prolonged longeron shadowing during a Soyuz undocking. Analytical reconstruction of induced thermal and dynamic structural loads showed an exceedance of the mast buckling limit. Possible structural damage to the solar array mast could have occurred during this event. A Low fidelity video survey of the 2A mast showed no obvious damage of the mast longerons or battens. The decision was made to conduct an on-orbit dynamic test of the 2A array on December 18th, 2009. The test included thruster pluming on the array while photogrammetry data was recorded. The test was similar to other Dedicated Thruster Firings (DTFs) that were performed to measure structural frequency and damping of a solar array. Results of the DTF indicated lower frequency mast modes than model predictions, thus leading to speculation of mast damage.

A detailed nonlinear analysis was performed on the 2A array model to assess possible solutions to modal differences. The setup of the parametric nonlinear trade study included the use of a detailed array model and the reduced mass and stiffness matrices of the entire ISS being applied to the array interface. The study revealed that the array attachment structure is nonlinear and thus was the source of error in the model prediction of mast modes. In addition, a detailed study was performed to determine mast mode sensitivity to mast longeron damage. This sensitivity study was performed to assess if the ISS program has sufficient instrumentation for mast damage detection.

Keywords Non-linear • Modal analysis • Photogrammetry • Damage detection

1.1 Introduction

The on-orbit construction of the International Space Station (ISS) began in November 1998, and was completed in July of 2011. The ISS consists of eight solar arrays for power generation. Each array is mounted on a rotating gear box for solar tracking and is deployed with a four longer on mast. Each mast is made of 32 bays consisting of longerons, fixed battens, flexible battens, and cable diagonals. Early in the ISS assembly process it was noted that thermal and dynamic conditions exist that could buckle a solar array mast longeron. This condition exists when one longeron is shadowed by another structure, thus causing asymmetric thermal loading in the mast longeron.

The ISS program developed a software tool to predict longeron shadowing events and to minimize periods of extreme loads. During the 19S Soyuz undocking December 1, 2009, the vehicle was in a long period of solar array longeron shadowing. The analysis predicted extreme loads in array 2A longeron and possible buckling. It was determined that an on-orbit test should be performed to analyze the dynamic response of the 2A array to check for damage.

This test produced a significant frequency difference in the first In Plane Array Mode compared to the analytical model and the other arrays. The ISS program requested a complete analysis of this event to determine if the 2A array was damaged

M. Laible (✉) • K. Fitzpatrick
The Boeing Company, 3700 Bay Area Blvd., Houston, TX, USA
e-mail: michael.r.laible@boeing.com; kristin.l.fitzpatrick@boeing.com

M. Grygier
NASA, Johnson Space Center, Houston, TX, USA
e-mail: Michael.S.Grygier@nasa.gov

G. Kerschen et al. (eds.), *Topics in Nonlinear Dynamics, Volume 1: Proceedings of the 31st IMAC, A Conference on Structural Dynamics, 2013*, Conference Proceedings of the Society for Experimental Mechanics Series 35,
DOI 10.1007/978-1-4614-6570-6_1, © The Society for Experimental Mechanics, Inc. 2013

or not. This paper documents the analysis performed and investigates possible solutions to the dynamic differences of this array. In addition to the dynamic analysis, analysis was performed to determine if a longeron did fail, can the failure be detected from existing on-orbit instrumentation.

Section 1.2 of this report presents the background of longeron shadowing and the specific 2A longeron shadowing event. Section 1.3 describes both the linear and nonlinear 2A array modal analyses performed and a comparison to the other ISS arrays. Section 1.4 outlines the analysis performed to determine if we can detect mast damage utilizing the instrumentation on-board ISS. Section 1.5 discusses the conclusions.

1.2 Problem Description

1.2.1 ISS Array Longeron Shadowing

The ISS has eight solar arrays, each consisting of a mast, two solar cell blankets, and four blanket boxes. These masts are attached to the Beta Gimbal Assembly (BGA) and can rotate independently about the long axis of the mast. Figure 1.1 illustrates the ISS configuration with the eight arrays rotated independently and the 2A Array; the focus of this paper.

Each mast is made up of four longerons as shown in Fig. 1.2. If one longeron is shadowed and the others heated, two longerons will be in compression and others will be in tension. This can cause buckling of the longerons. Typical buckling and temperature values are shown in Fig. 1.2.The buckling starts at a combined dynamic and thermal load of 1,340 lbs [1].

The ISS program performs a detailed longeron shadowing analysis and values are reported real-time. The ISS mission operation personnel will receive a warning if a longeron is shadowed and loads are at max limit values. When 1the warning is received the BGA is rotated to eliminate longeron shadowing.

1.2.2 2A Anomoly

During an ISS maneuver in December, 2009, the 2A Array experienced Longeron Shadowing for an extended period of time. Post flight analysis proved that the limit load was exceeded and that buckling could have occurred. To ensure structural integrity a detailed photo review was performed with no noticeable damage reported.

The ISS program then determined that a Dedicated Thruster Firing (DTF) test should be performed on the 2A Array to determine the modal structural properties. Instrumentation does not exist on the array mast itself; therefore, photogrammetry data was recorded and analyzed to determine the modal parameters of the array. The Image Science and Analysis Group (ISAG), at NASA JSC received analog video taken during the 2A DTF from two ISS external cameras [2]. Figure 1.3 illustrates the camera views and jet plume direction toward the 2A Array. The thruster firing lasted for 1 s and was designed to excite the modes of the 2A Array.

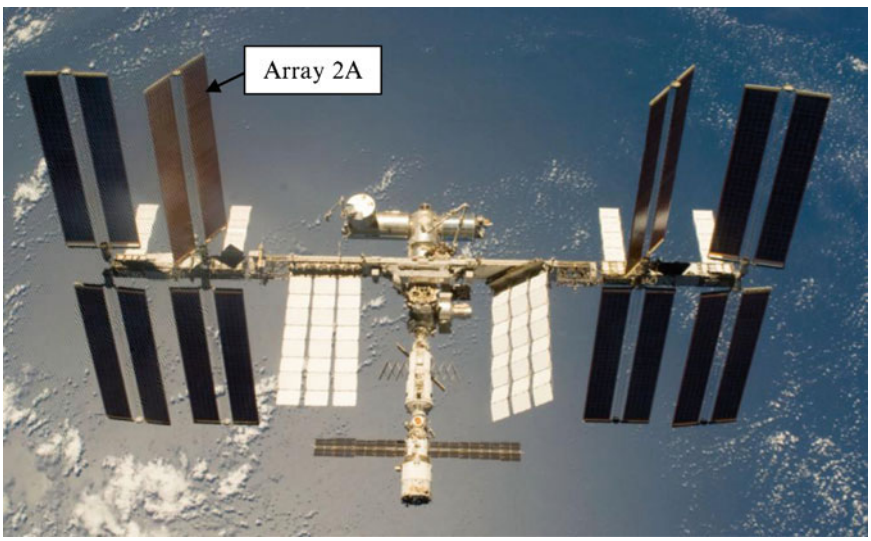

Fig. 1.1 International space station assembly complete

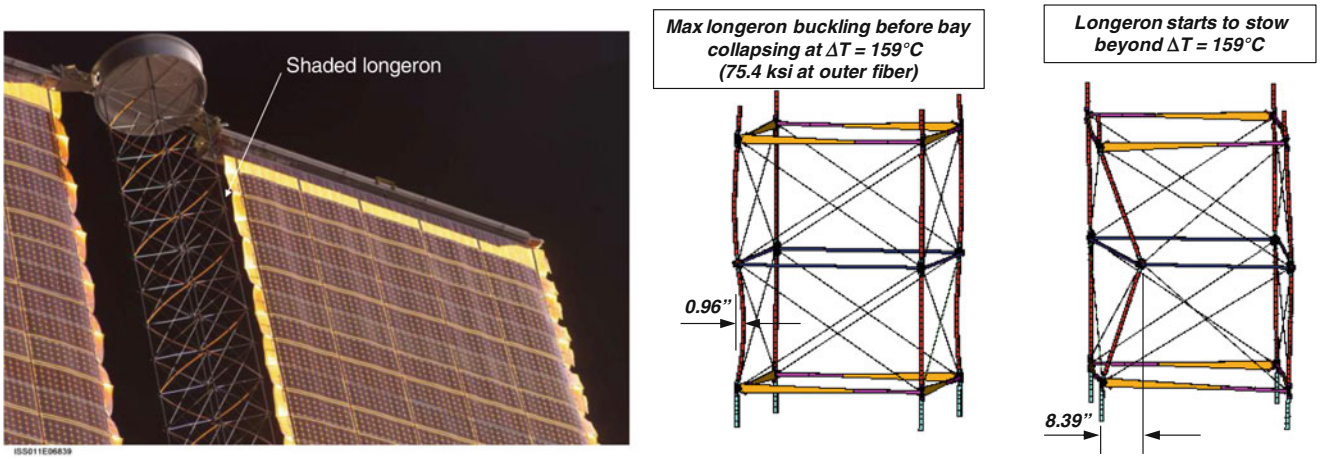

Fig. 1.2 Solar array shadowing and thermal buckling

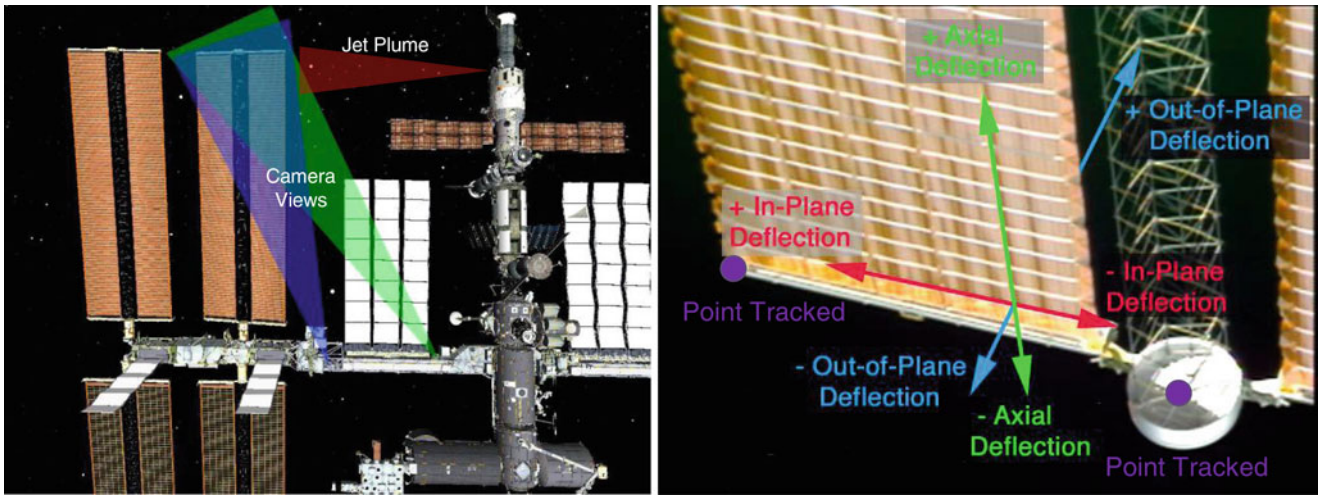

Fig. 1.3 ISS camera views, jet plume and photogrammetry coordinate frame

The ISAG used their image processing software to track two points at the end of the 2A Solar Array Wing (SAW), Fig. 1.3. One point was on the mast cap located at the end of the mast of the solar array. The second tracked point was on the tip of the blanket box at the end of the solar array. The motion of each point was tracked in the video recorded from each of the two cameras and used to compute the relative displacement of the SAW tip in each axis, defined by the plane of the array during the DTF. Due to the high mathematical correlation between the axial and out of plane motion, the calculations were conducted in a way which constrains the axial position to a fixed value of 0. This constraint is acceptable given that the motion of the array in the axial direction is significantly less than the In Plane (IP) or Out Of Plane (OOP) motions. The major modes observed from this DTF and previous DTF's are the first OOP and first IP modes. The frequency of the OOP and IP modes found for other arrays are between 0.06–0.0675 Hz and 0.09–0.099 Hz, respectively.

When the photogrammetric analysis was completed, the time history data was low-pass filtered and the FFT was also computed. The OOP frequency was within the expected range but the IP frequency was 14% lower. The displacement time history and FFT of the array mast cap is illustrated in Fig. 1.4.

The Eigensystem Realization Algorithm (ERA) [3] was utilized to extract the modal parameters from the detrended photogrammetry data sets. The Modal Assurance Criterion (MAC) was calculated between the extracted mode shapes and the analytical model mode shapes. The comparison results between the extracted modal parameters from the data and the analytical modal parameters are summarized in Table 1.1. The frequency of the first OOP test mode matched within 5% of the first 2A OOP analytical mode. The frequency difference between the first IP test mode and IP analytical mode ranged from 14 to 17%.

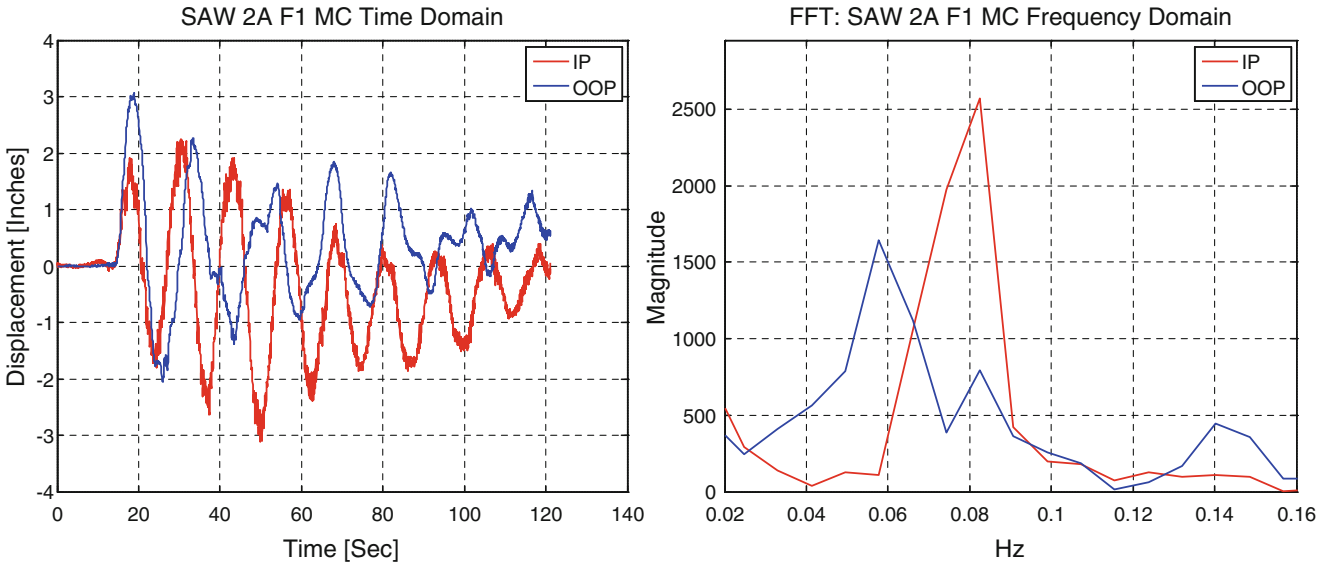

Fig. 1.4 Mast cap displacement time history and FFT

Table 1.1 2A array test modes versus analytical model modes

Test data				Analysis data				
Mode #	Freq (Hz)	Damp (%)	EMAC (%)	Mode #	Freq. (Hz)	Freq. diff (%)	MAC	Mode description
				9	0.0597	2.68	0.951	All SAWs OOP
				10	0.0613	0.0	0.948	All SAWs OOP
1	0.0613	4.6	92.42	12	0.0648	−5.40	0.942	Port SAWs OOP
				14	0.0651	−5.84	0.943	Port SAWs OOP
				16	0.0665	−7.82	0.940	Port SAWs OOP
2	0.0798	3.3	96.12	17	0.0933	−14.47	0.909	Port SAWs IP
				19	0.0964	−17.22	0.904	Port SAWs IP
				22	0.0971	−17.82	0.902	Port SAWs IP

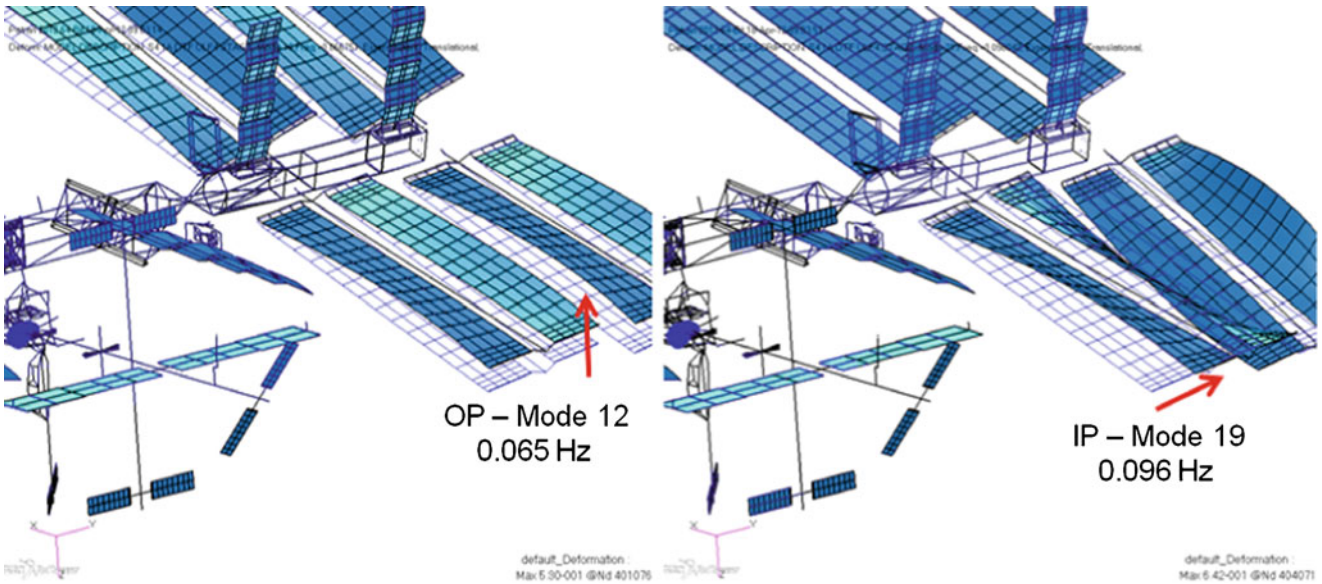

Fig. 1.5 Analytical array out of plane and in plane

Figure 1.5 illustrates the analytical mode shape of the OOP and IP modes. The figure is the MSC PATRAN model of the ISS system model, zoomed in on the 2A array. The mode number and frequency is shown for the OOP and IP 2A array modes.

1.3 2A Array Modal Analysis

The 2A Solar array had experienced a sustained longeron shadow event. The analytical reconstruction of the event showed an excedence in the limit loads when combining the dynamic and thermal loads. An on-orbit dynamics test was performed and the IP mast mode was found to be 14% lower than what was expected when compared with the analytical dynamic model. In addition, the first IP 2A Array test mode was lower than what was previously seen with any other array on-orbit test. The large frequency difference between the IP test and analytical mode was a concern to the program and resulted in the request of a more detailed analysis to determine the cause of the difference.

The following detailed analysis was conducted to determine why the first IP Array mode was lower and if damage of the array could be detected with modal analysis.

1.3.1 Linear Analysis

The ISS loads system model is made up of over 90 super elements and has 35,000 dof. Each model takes about 60 min of computer time for the SOL 103. When performing time domain solutions (SOL 109 or 129) the time increases dramatically. This is an unmanageable model when performing parametric runs and numerous failure analysis time domain runs. To simplify the problem, a stiffness matrix was developed using the NASTRAN DMIG option with the boundary conditions being constrained at the approximate CG of the ISS and the other boundary being the four grids that the Solar array BGA attaches to ISS.

In addition, the solar array model used during nominal loads analysis has a simplified mast (one Center Bar, ten pieces) and did not model the individual longerons. To perform parametric studies of failed longerons the detailed mast model would have to be integrated into the simplified system model. Figure 1.6 illustrates the baseline loads model (left) and the detailed mast model delivered from the developer (right). The highlighted CBARS are the longerons used for the failed analysis. The far right is a close up of the longeron model and cross battens. In failed longeron cases the complete connection is removed at positions depicted in Fig. 1.6 (MID and BASE).

The detailed array model was compared against the simplified baseline array model. A modal solution was performed with both models being constrained at the base coordinate frame as shown in Fig. 1.6. The frequency differences between the modes of each model were all within a $1/2\%$. Once the model comparison was complete the detailed mast model was attached into the station stiffness and sensitivity studies were performed. Figure 1.7 illustrates the station stiffness model with the detailed mast and array models.

The first run was the SOL 106, a non-linear solution, which involved pulling the blankets tight to the baseline spring tension. The blanket elements were pre-stressed in order to account for the effect of the blanket tension load. The blanket tension load was analyzed using geometric non-linear static analysis sequence (NASTRAN SOL 106) [4]. The differential stiffness matrix and coupled mass matrix are used in normal mode analysis solution sequence (NASTRAN SOL 103) and the EXTSEOUT card to build the DMIG of the array, PCH and ASM files. This is performed by restarting the SOL 106 run and using the EXTSEOUT card.

Now the ISS system model can be replicated by a NASTRAN run using the ISS DMIG, Solar array DMIG, and detailed four-bar BGA assembly. The time domain and modal solution runs could be performed with minimum computer time. Again this model is shown in Fig. 1.7 which also notes the chosen failed longerons for the analysis. These longerons were chosen from a separate analysis, which showed that these areas are the most likely to fail.

The Boeing Loads and Dynamics group performs thruster plume analysis on all station arrays. The program that performs the analysis uses plume jet mass flow and impinges on individual plates modeling the array. The output is a force on each individual grid. The program has been validated with other array displacement checks. A special routine was developed to map force values and vectors for each array blanket. These force values were mapped to every array blanket and the mast cap. The array wing displacement was plotted and compared to the on-orbit data. These comparison plots are shown in Fig. 1.8. As can be seen by the displacement time history plots, the frequency of the on-orbit data and analytical data does not compare for the IP mode. This also was seen in the frequency domain.

In addition to the time domain runs, a parametric study was performed using the modal solution. Several models were created to conduct the parametric study; the Baseline array (BL 081), Baseline array with MID longeron partially failed

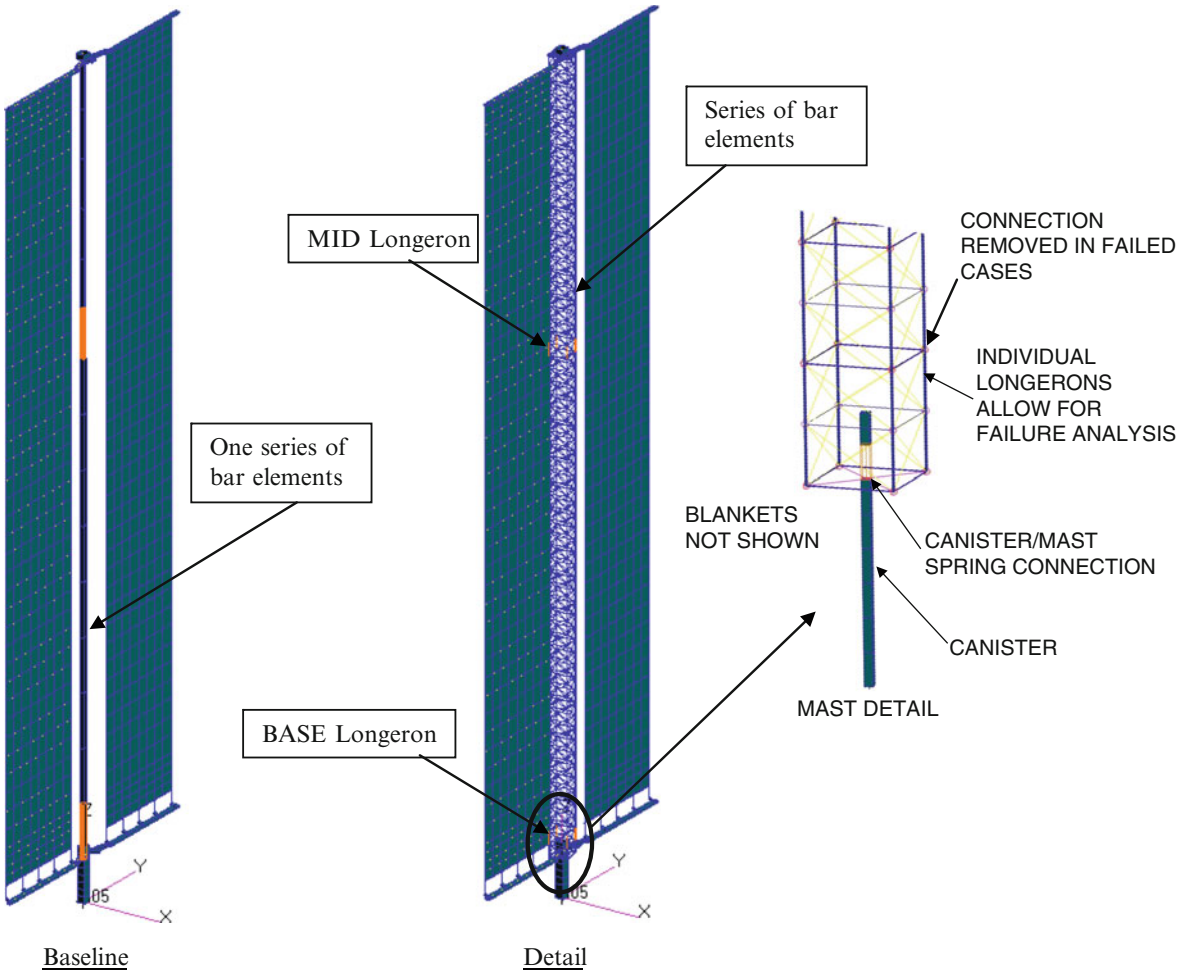

Fig. 1.6 Baseline versus detailed array model

(BL 081 MD1) and total fail (BL 081 MD1 TL), and the base longeron partially failed (BL 081 BS1) and base longeron totally failed (BL 081 BS1 TL). The results of this parametric study are shown in Table 1.2. As can be noted the Base longeron totally failed still shows a 10% frequency difference from the on-orbit test IP frequency.

These results indicate that the on-orbit IP frequency difference between the on orbit test and the analytical model cannot be explained by a longeron failure alone. Other areas had to be investigated.

After a more detailed look of the system, it was determined that the IP mode stress was greatest in the four-bar linkages, which attaches the BGA to the ISS truss. In fact, the first two modes are dominated by the four-bar/BGA assembly. A detailed picture of the four-bar assembly is shown in Fig. 1.9.

1.3.2 Non-linear Analysis

To get a better understanding of the four-bar assembly mechanism and the inherent non-linearities, the ground test documents were reviewed. The ground test data illustrated an initial slippage followed by a high degree of bi-linearity, most notably between the ± My cases. Figure 1.10 shows the strain gauge location and the derived moment output from the My input. The test data showed that some of the deflections were different in the plus and minus loading cases. Within each load case, the deflection verses load curves were relatively linear, but two curves emerged in some of the plus and minus load cases that were not (My shown in Fig. 1.10) [5–7].

This observation in the ground test data means that there was uneven slippage in some of the four-bar to clevis connections. After ten iterations of the ground test the best agreement between the model and linear data required stiffness values be

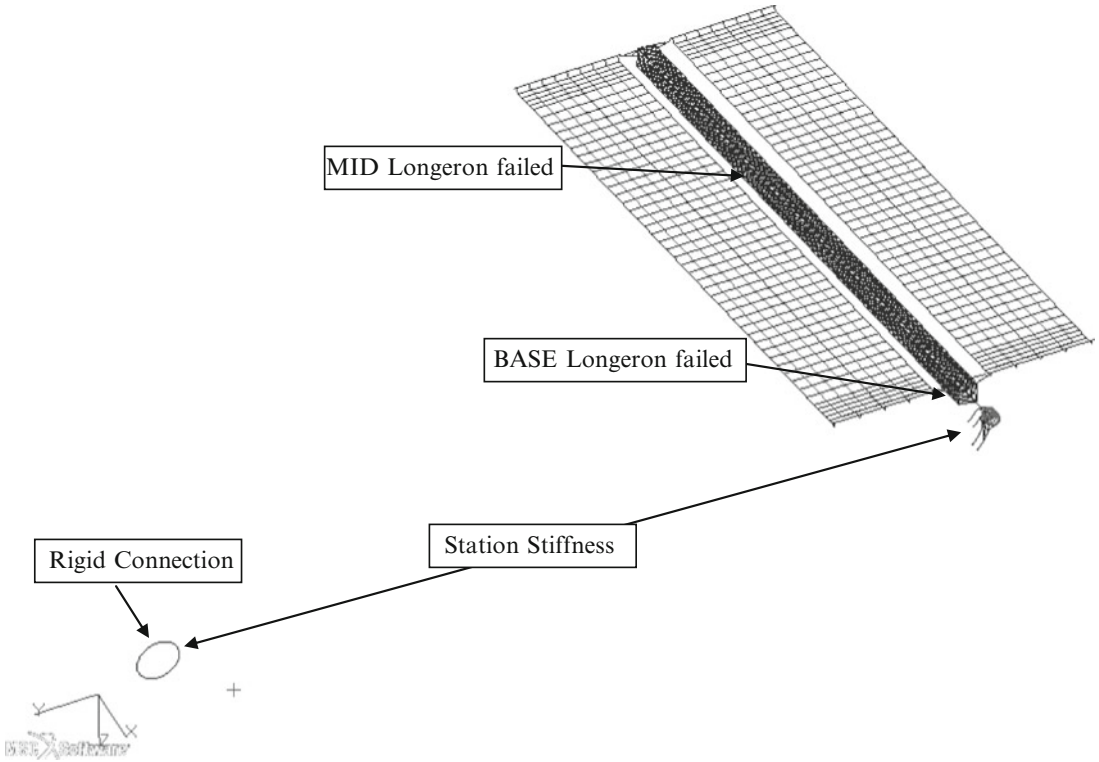

Fig. 1.7 ISS stiffness with detailed BGA and array model

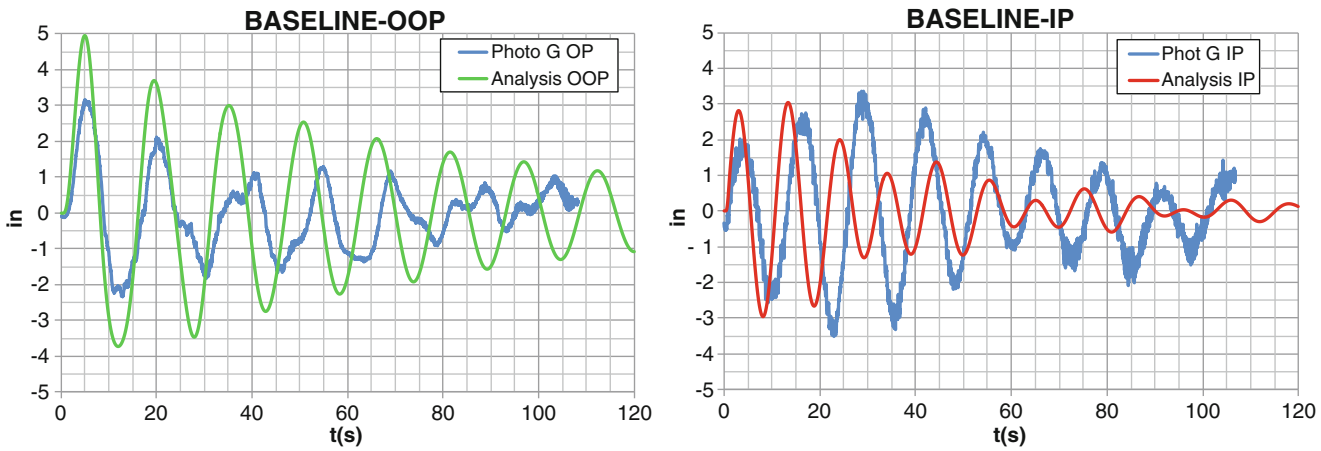

Fig. 1.8 Time domain comparison of out of plane and in plane test and baseline analytical data

Table 1.2 Array frequency comparison

Mode description	2A DTF	BL 081	% diff test	BL 081 MD1	BL 081 MD1 TL	BL 081 BS1	BL 081 BS1 TL	% diff test
OP	0.0602	0.0649	8	0.0646	0.0644	0.0635	0.0634	5
IP	0.0814	0.0969	17	0.0929	0.0926	0.0903	0.0898	10
TOR & IP	0.103	0.0934	−10	0.0957	0.0953	0.0945	0.0945	−9
Mast OP	0.152	0.1519	0	0.1519	0.1519	0.1517	0.1517	0

adjusted in the model four-bar to clevis springs, Mx (in-lb) = 450,000 to 900,000, My (in-lb) 650,000 to 2,280,000, and Mz (in-lb) 600,000 to 6,000,000. These new stiffness values were developed to correlate to the linear slope of the test data, thus the model is expected to be stiffer.

All reports indicate that the non-linearities are mechanism slippage and are in the four-bar to IEA clevis connection.

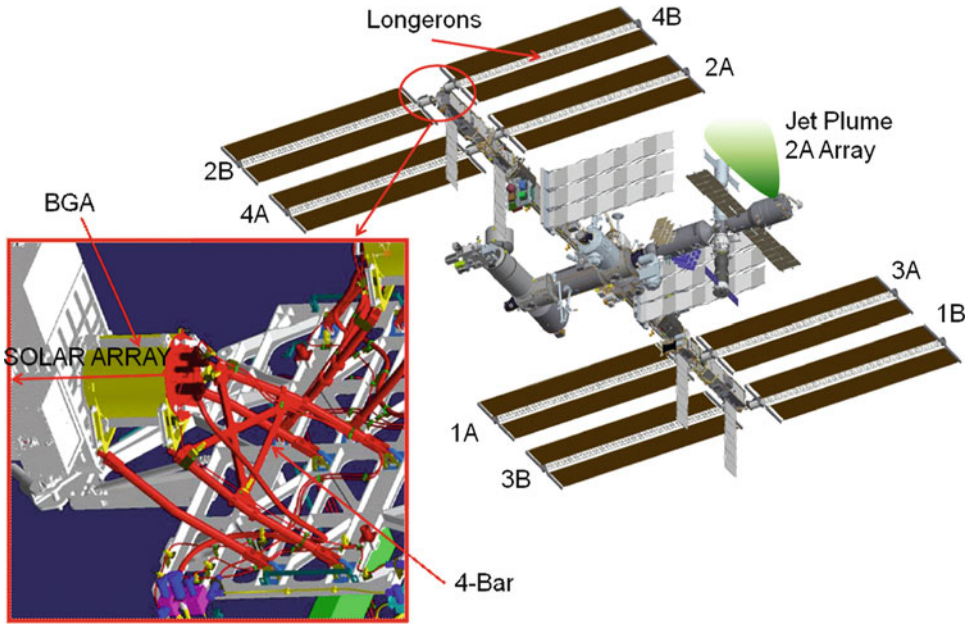

Fig. 1.9 ISS four-bar assembly

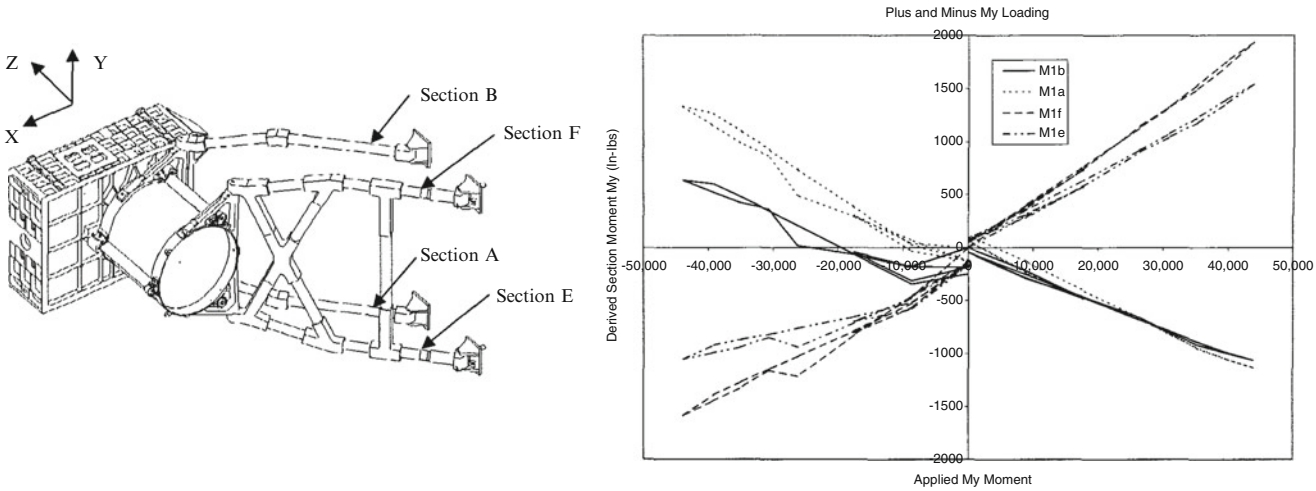

Fig. 1.10 Ground test four-bar assembly and ground test stiffness data

The ground test documents showed that non-linearities exist in the four bar connections. As noted earlier, the four-bar connections dominate the first two modes, OOP and IP. At this point a more detailed analysis was performed on the on-orbit data using the Boeing Test Analysis Correlation Solutions (BTACS) program. The BTACS system identification tool includes a method that extracts modal parameters within a set window over a prescribed period of time within the data set. The photogrammetry displacement data was analyzed using the system identification tool of the BTACS program. The modal parameters were computed every 0.67 s using a window of 60 s of data.

The frequency values, of the extracted modes, were then plotted for each time increment where the color of the data point represented the EMAC value, red being greater than 90% and orange greater than 80%. Figure 1.11 shows the results of the BTACS system identification analysis of the on-orbit data array data showing non-linearities of the first OOP and first IP Modes. The frequency of the OOP mode ranged from 0.06 to 0.068 Hz and IP 0.079 to 0.09 Hz over time, as the amplitude of the array displacement diminished.

To better understand the mechanism of the four-bar clevis to truss connection, on-orbit photos were reviewed. As previously noted the ground test documents indicate that the non-linearities were most likely coming from the four-bar to truss clevis connection. Figure 1.12 depicts the on-orbit photos showing the placement and close-up of the four-bar to clevis connection.

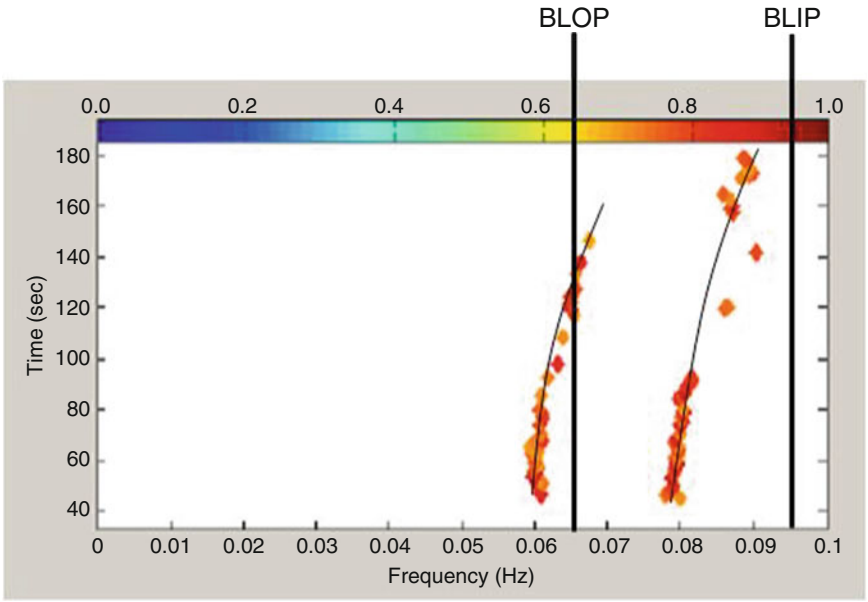

Fig. 1.11 Photogrammetry data mode frequencies vs time

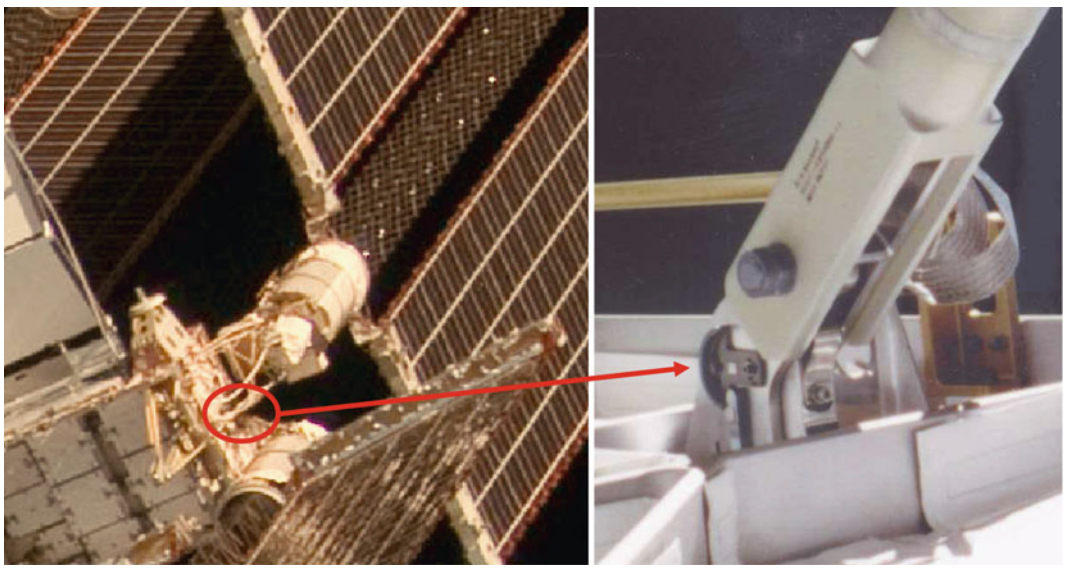

Fig. 1.12 Four-bar to truss mechanism

Table 1.3 BGA to truss spring values

	Baseline (in-lb)	Ground test – BL 081 (in-lb)	Modified – BL 081 DOF 1,3,5 front (in-lb)
CELAS2 DOF1	5,500,000	5,500,000	5,000
CELAS2 DOF2	5,000,000	5,000,000	5,000,000
CELAS2 DOF3	300,000	300,000	5,000
CELAS2 DOF4	450,000	900,000	900,000
CELAS2 DOF5	650,000	2,280,000	2,280
CELAS2 DOF6	600,000	6,000,000	6,000,000

Figure 1.12 illustrates the pin mechanism that locks the four-bar in the extended position (far right). This pin connection is modeled as a set of springs in the BGA detailed NASTRAN [8] model. During the ground test it was decided to correlate the model to the linear stiff portion of the test data, thus increasing the rotational spring values as shown in Table 1.3, Colum 3 (Ground test BL 081). The original values of the model are shown in column 2 (Original).

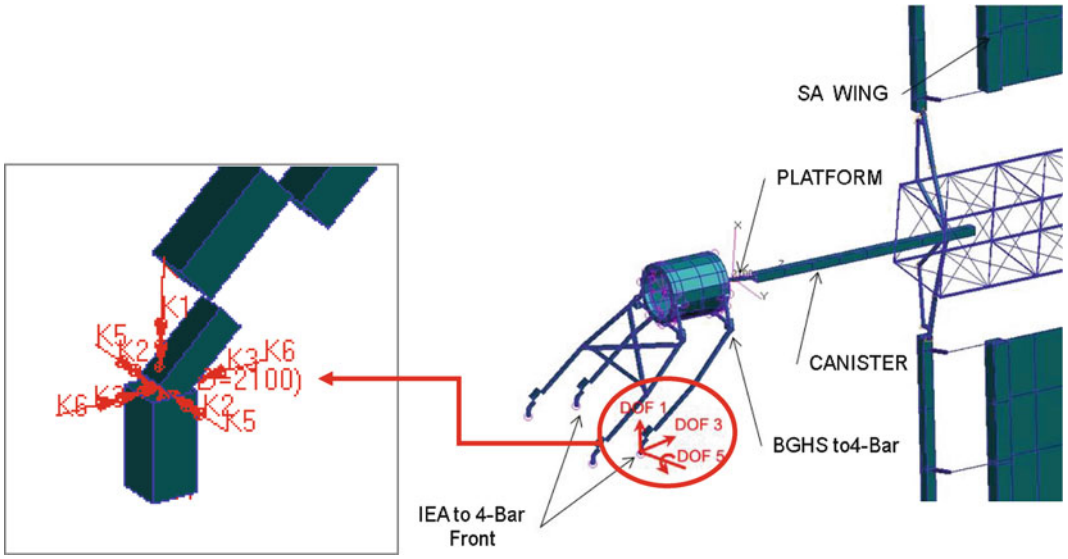

Fig. 1.13 Modified BGA description

Table 1.4 Analytical results of modified BGA

On-orbit test		BL 081 (Hz)	% diff test	BL 081 DOF 1, 3, 5 front (Hz)	% diff test
0.0602	OOP	0.065	8	0.061	1
0.0814	IP	0.097	17	0.079	−3
0.103	TOR	0.096	−7	0.096	−7
0.152		0.152	0	0.151	−1

Table 1.5 GAP stiffness values

	GAP Disp (in)	GAP closed stiffness (in-lb)	GAP open stiffness (in-lb)
DOF1	0.00005	5,500,000	5,000
DOF2	No gap	5,000,000	5,000,000
DOF3	0.0001	300,000	5,000
DOF4	No gap	900,000	900,000
DOF5	No gap	2,280	2,280
DOF6	No gap	6,000,000	6,000,000

A series of NASTRAN runs were performed modifying the four-bar to truss spring values. It was found that modifying the front two connections in DOF 1, 3, and 5 (see Fig. 1.13) would impact the frequency of the IP mode while having negligible effects on the frequency of the other modes. Column 4 of Table 1.3 contains the final spring values used for the analysis.

After all the runs with spring reductions were complete, the final OOP and IP mode frequency values were checked against the baseline mode and the on-orbit test. Table 1.4 illustrates the final frequency values and the percent frequency difference from the on-orbit test. The modified spring values changed the frequency of the IP mode without affecting the frequency other modes. These results allowed for a plausible explanation of the modal discrepancies of the IP frequency difference. It must be noted that this is a linear solution and that we saw non-linear results from the on-orbit test.

To account for the non-linear results seen in the on orbit photogrammetry data, GAP elements were used for the four-bar to truss clevis connection. The solution 129 was used for this analysis. Numerous runs were performed using GAP elements and the NOLIN card. The final analysis was performed using the NASTRAN GAP elements with varying axial stiffness values depending on open or closed gap. To model the on-orbit structure the stiffness was modeled to be less with an open gap. The closed gap stiffness is the same as the baseline A recap of the GAP card values are shown in Table 1.5.

The GAP elements were used on the four-bar to truss clevis on the front locations only. The initial gap open was determined by performing nominal plume runs and plotting the relative displacement between the GRIDS with the baseline spring constant. The exact GAP opened value was determined after several runs and acceptable results were achieved.

Once the proper GAP parameters were achieved, a time domain SOL 129 was performed. When performing non-linear transient analysis, the damping value is specified with the W3 parameter and is the damping at a specified mode. The frequency used for this was a split between OOP and IP mode and was valued at 2%. The comparison time domain of the

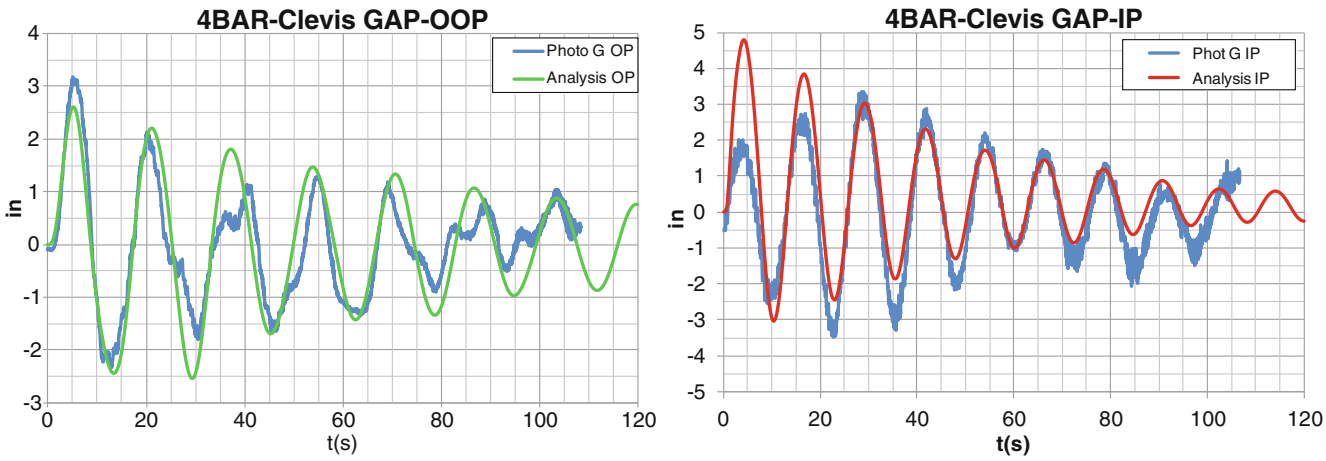

Fig. 1.14 On-orbit versus analytical non-linear time domain data

Fig. 1.15 Relative displacement of front four-bar clevis

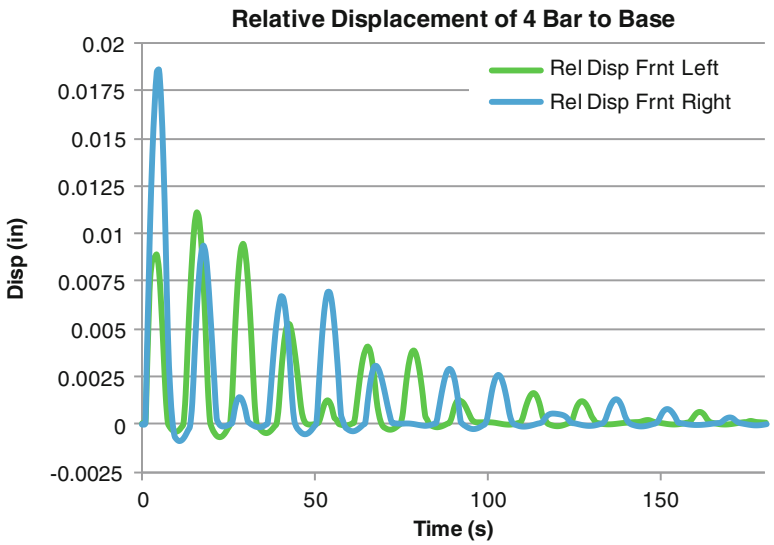

on-orbit test data and the non-linear analytical data is shown in Fig. 1.14. As can be noted the comparison is much better than the baseline (Fig. 1.8) and considered to be a good analytical representation of the on-orbit structure.

In addition to the time domain of the individual OOP and IP displacement of the array, the overall relative displacement of the spring grids were plotted. Figure 1.15 shows the relative displacement of the front four-bars to truss clevis. The maximum displacement is 0.0175". This displacement is a little more than double the complete tolerance stack up of the four-bar mechanism. The tolerance stack up of the four-bar clevis to truss connection is 0.0073".

For a 'quick look' analysis the softened springs were used on the boundary connections of the starboard truss IEA super element and the 2A BGA super element in the full detailed ISS system model. This model has all eight arrays thus it will have eight OOP modes, eight IP modes, and eight torsional array modes.

Table 1.6 compares the system model baseline modes and the 2A array reduced boundary connection model modes. It is noted, in bold, the 2A IP array mode of the modified model is lowered by the amount seen on-orbit. The mode shape comparison of the test modes and the modified model modes matched, and with the lower frequency value, would have deemed the array nominal if this was in the original analytical model when compared to on orbit 2A DTF.

1.4 Mast Damage Sensitivity Study

In addition to the analysis performed to investigate the array mode frequency difference, it was asked if the current ISS instrumentation would allow for mast damage to be detected. A detailed study was performed to investigate if a longeron failure could be detected with current instrumentation.

Table 1.6 ISS modal comparison of baseline and modified

Baseline mode (Hz)	Mode description (baseline)	DOF 135 mode (Hz)	Mode description (modified)	% diff
0.05973	OOP PORT/STBD	0.05884	OOP PORT/2A	−1.5
0.06134	OOP PORT/STBD	0.06071	OOP PORT/STBD	−1.0
0.06472	OOP STBD	0.06472	OOP STBD	0.0
0.06484	OOP PORT/2A	0.06294	OOP PORT/2A	−3.0
0.06499	OOP STBD	0.06499	OOP STBD	0.0
0.06511	OOP PORT	0.06497	OOP PORT	−0.2
0.06566	OOP STBD	0.06566	OOP STBD	0.0
0.06648	OOP PORT	0.06628	OOP PORT	−0.3
0.09333	IP PORT sym	**0.08128**	**IP 2a**	**−14.8**
0.09566	IP STBD sym	0.09568	IP STBD sym	0.0
0.09639	**IP PORT/2a**	0.09473	IP PORT sym	−1.8
0.09664	IP STBD anti-sym	0.09664	IP STBD anti-sym	0.0
0.09676	IP STBD	0.09676	IP STBD anti-sym	0.0
0.09707	IP PORT, STBD anti-sym	0.09700	IP PORT anti-sym, STBD	−0.1
0.09713	IP PORT anti-sym, STBD	0.09713	IP PORT, STBD anti-sym	0.0
0.09812	IP PORT anti-sym	0.09811	IP PORT anti-sym	0.0
0.09961	TOR STBD	0.09961	TOR STBD	0.0
0.09968	TOR STBD	0.09968	TOR STBD	0.0
0.09974	TOR STBD	0.09974	TOR STBD	0.0
0.09976	TOR PORT	0.09978	TOR PORT	0.0
0.09977	TOR STBD	0.09977	TOR STBD	0.0
0.09995	TOR PORT	0.09967	TOR PORT	−0.3
0.10025	TOR PORT	0.10022	TOR PORT	0.0
0.10036	TOR PORT	0.10036	TOR PORT	0.0

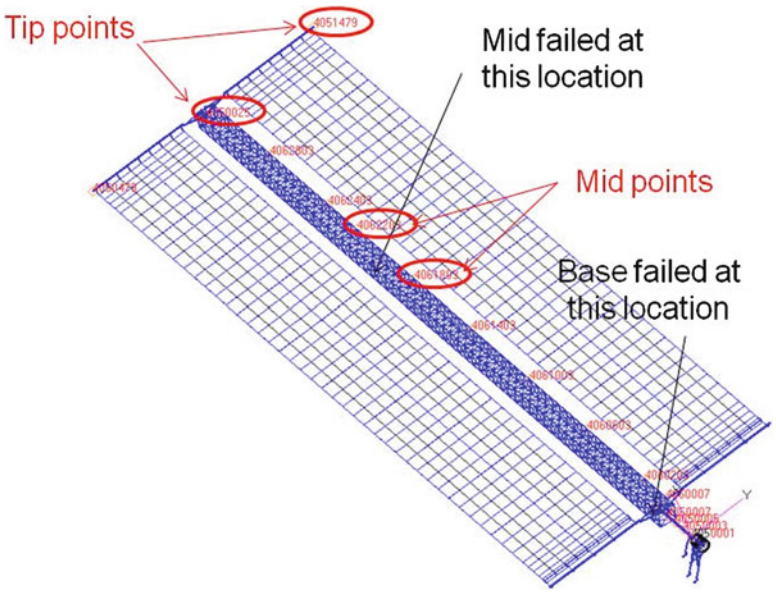

Fig. 1.16 Array camera viewing locations

The only instrumentation on orbit to measure ISS array modes is the photogrammetry system. The photogrammetry analysis needs at least two cameras on each area being investigated. It is possible but very difficult to get four cameras dedicated for an array test. For this study it was decided to use four cameras. Figure 1.16 illustrates the two areas the cameras would be pointed, one set at the tip and one set at the midpoint, spanning the most credible failure area.

A set of SOL 103, modal solution, runs were performed on the baseline array model, failed at mid model, and failed at base model. The modal parameters for each model was output and compared to the baseline model modal parameters. For each run the frequency difference and MAC was calculated. The baseline model has over 700 modes from 0 to 5.5 Hz. To reduce the amount of modes to investigate, only modes containing 2% or greater kinetic energy in the array mast were saved. This reduced the problem down to 60 modes. It also must be mentioned that this is a total failure of the longeron and does not assume partial fractures.

Table 1.7 BGA at 81° damaged at MID

Nom freq	Fail freq	MAC	% diff freq	Mode description	% KE mast
0.093	0.090	0.758	−3.2	Torsion	3
0.6777	0.6247	0.823	−7.8	Mast bending with blanket (anti) bending	5
1.5107	1.259	0.745	−16.7	Out plane bending with lower blink box	20
1.5107	**1.2868**	**0.722**	**−14.8**	**Added mode from mid damage**	**20**
2.3272	2.2607	0.752	−2.9	Good first in plane bending	24
4.344	4.06	0.642	−6.5	45° plane second bending	2
4.3824	4.6232	0.545	5.5	Out plane second bending	52

Table 1.8 BGA at 81° damaged at base

BL freq	Fail freq	MAC	% diff freq	Mode description	% KE mast
0.093	0.090	0.758	−3.4	Torsion	19.2
1.001	0.980	0.924	−2.1	Mast in plane first bending	9
2.327	2.254	0.984	−3.1	Good first in plane bending	24
4.344	4.083	0.602	−6.0	45° plane second bending	2
4.382	4.083	0.915	−6.8	Out plane second bending	52

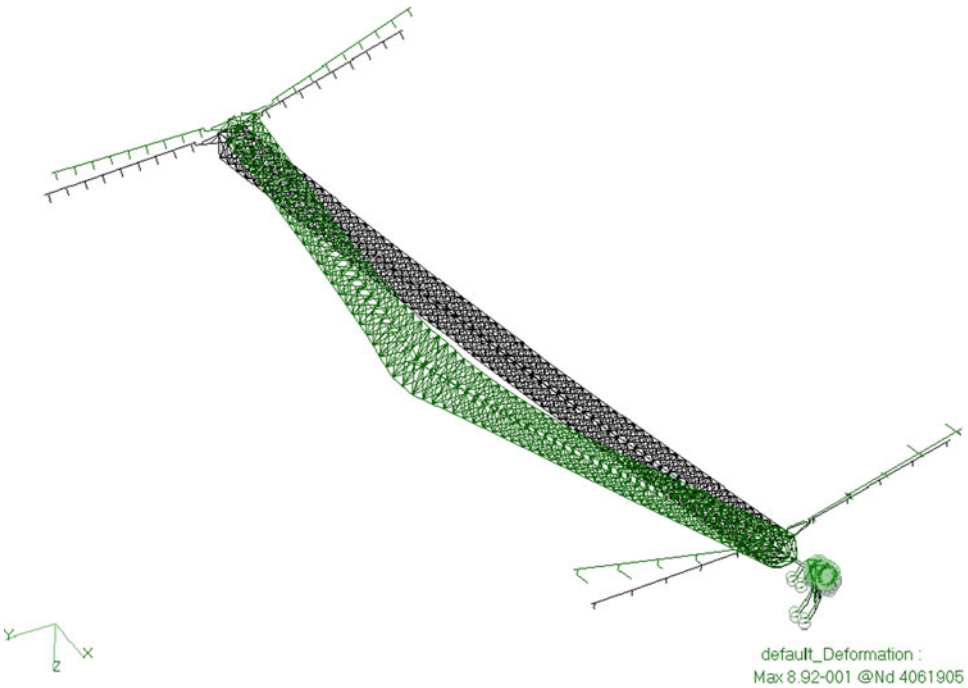

Fig. 1.17 Mast mode shape comparison with MID longeron failure

Once the major modes were selected, the MAC was calculated using the four grids as noted in Fig. 1.16. Table 1.7 summarizes the data results for the mast failed at mid model and Table 1.8 summarizes the data for the mast failed at base model.

Table 1.7 is the summary of the failed longeron at the mid point of the mast. The torsion mode has a low MAC between the baseline and damaged model but it would be difficult to detect this with the cameras available and determining if this is the results of the four-bar contribution or mast damage. The next possible mode for detecting mast damage was the 0.677 Hz mast bending mode. The failed mast does show a lower MAC value and mode frequency. The best possibility of damage detection is the additional mode in the failed case at 1.2868 Hz (highlighted in bold). When performing the MAC the best match is the baseline mode at 1.5107 Hz. This mode would be the best mode to detect a total longeron failure at mid mast and the comparison mode shape is illustrated in Fig. 1.17. Some other modes exist above 4 Hz but it is difficult on orbit to physically excite modes at that high of a frequency and the reliability of photogrammetry to capture the modes at that frequency is unknown, due to the frame rate of the cameras of 15 or 30 Hz.

Table 1.8 illustrates the frequency difference and MAC values between baseline model and the failed longeron at the base of the mast model. Once again the first torsion mode may be difficult to determine if the difference is caused by the mast

or four-bar damage but with the higher KE it should be easier to excite on orbit. The modes above 4 Hz seem to have the best chance of detecting mast damage, but again the modes at this high a frequency are difficult to excite on orbit and it is unknown if modes in this frequency range can be reliably detected using photogrammetry.

The final conclusions are that a mast failure can be detected with modes above 1 Hz for MID failure and above 2 Hz for the base failure. The limitation of the mast failure detection using existing photogrammetry is the ability of only having two areas to track. Mode shape differences are easier to detect when tracking four or more areas. An exhaustive study of the optimal tracking areas was not performed and could be an area of improvement. In addition, the program is developing high definition cameras that would enhance the detection process but would still be limited to tracking only two areas.

1.5 Conclusions

The 2A ISS array was subjected to extreme limit loads from a longeron shadowing event. The longeron shadowing event may cause a thermal buckling of the longeron on the ISS solar array mast. To check for structural integrity of the array, a photo survey was conducted and an on-orbit modal test was performed. No damage was found from the photo survey but the on-orbit modal test showed a frequency difference in the first IP Array mode. Through analysis it was found that this frequency shift could not be explained by mast damage alone, but in fact may be a non-linear characteristic of the BGA four-bar clevis to truss attachment. Modal solutions proved that by softening the front four-bars that the first IP mode frequency was lowered without affecting the other modes' frequencies. This was exactly what was observed in the on-orbit test. A simplified station model was developed with the detailed solar array model to perform time domain NASTRAN runs. The time domain runs were performed with the soft front four-bars with good results but still was not matching the on-orbit data.

It was found that the on-orbit 2A array displacement data increases in frequency as displacement amplitude decreases. This indicates a non-linear mechanism. This non-linear phenomenon was modeled using NASTRAN gaps with the baseline stiffness of the front four-bars when the Gap was closed and when it was opened the soft spring values were applied. The time domain displacement results matched the on-orbit test. It was concluded that the non-linearities could be attributed to gaps, gaps with pre-loads, and thermal effects. It was also determined that if a longeron on the array mast was damaged, completely separated, that it would be difficult to measure with current instrumentation, but with additional and higher quality cameras, it would be possible.

References

1. Solar array mast buckling report, ATK Space Systems 1163D3883, 10 June 2010
2. P4-2A photogrammetry results, NASA-JSC-Image Science and Analysis Group, 5 Jan 2010
3. Juang JN, Pappa RS (1985) An eigensystem realization algorithm for modal parameter identification and model reduction. J Guid 8(5):620–627
4. Space station PG-2 fully deployed solar array nastran dynamic model, EM NO. SSSA57, Lockheed Martin Missiles and Space, C. C. Tang, 10 Feb 1997
5. BGA static test on-orbit deployed loads model correlation, Boeing Memorandum EID-05475, 6 April 2000
6. BGA on-orbit static test/Finite element model correlation, Boeing Memorandum EID-05379, 18 April 2000
7. Qualification mast canister stiffness, strength, and structural alignment test report, Lockheed 518D972, 24 May 1996
8. MSC/NASTRAN quick reference guide, MSC/NASTRAN, 2008

Chapter 2
Experimental Non-linear Modal Testing of an Aircraft Engine Casing Assembly

Dario Di Maio, Paul Bennett, Christoph Schwingshackl, and David J. Ewins

Abstract This paper aims to present experimental work on an aircraft engine casing assembly. Nowadays single components of casings can be modeled with such high accuracy that they can be validated by carrying out the model validation process using measured data from a sector of the entire assembly. This smart validation process can be achieved by carrying out the modal analysis with a Scanning LDV (Laser Doppler Vibrometer) system which allows good spatial resolution of the measured mode shapes. The validation process can be assumed valid under linear response conditions obtainable for low vibration amplitudes. Casings are typically connected together by joints which may or may not respond non-linearly under high levels of vibration. Therefore, prior to conducting any non-linear validation, the mode(s) responding non-linearly must be identified beforehand in order to correctly specify the non-linear modal testing required. The work presented here will use a large civil engine casing assembly comprising a Combustion Chamber Outer Casing (CCOC), High Intermediate Pressure Turbine Casing (HIPTC) and Low Pressure Turbine Casing (LPTC.) The Fine Mesh Finite Element Model (FMFEM) was successfully validated using linear modal analysis test data. One of the objectives of this work is to define the key points for conducting non-linear modal testing of such large casing assemblies and sub-assemblies. One outcome of the experimental work was a set of recommendations for performing measurements, which should be carried out within the frequency bandwidth selected during the model validation process. Experimentally derived non-linear response curves are presented in this paper.

Keywords Joints • Non-linear testing • Aircraft engine casing • Scanning LDV

2.1 Introduction

A civil aircraft engine casing assembly comprising a Combustion Chamber Outer Casing (CCOC), High Intermediate Pressure Turbine Casing (HIPTC) and Low Pressure Turbine Casing (LPTC) Fine Mesh Finite Element Model (FMFEM) was successfully validated using linear modal analysis test data [1] and (Private communication University of Bristol-Rolls-Royce). One of the objectives of this project was to define guide-lines for conducting non-linear modal testing of such large casing assemblies and sub-assemblies. The key aim was to produce a set of recommendations for performing measurements, which should be carried out within the frequency bandwidth selected during the model validation process. The validation process of the full assembly was performed using two measurement methods: (i) accelerometers and a roving instrumented impact hammer and (ii) using a Scanning Laser Doppler Vibrometry (SLDV) system and electromagnetic shaker. The first validation was carried out with the casing assembly supported vertically by bungees, whereas the second was tested with the assembly suspended horizontally.

D. Di Maio (✉) • D.J. Ewins
University of Bristol, Bristol, UK,
e-mail: dario.dimaio@bristol.ac.uk

P. Bennett
Rolls-Royce plc, London, UK

C. Schwingshackl
Imperial College London, London, UK

G. Kerschen et al. (eds.), *Topics in Nonlinear Dynamics, Volume 1: Proceedings of the 31st IMAC, A Conference on Structural Dynamics, 2013*, Conference Proceedings of the Society for Experimental Mechanics Series 35,
DOI 10.1007/978-1-4614-6570-6_2, © The Society for Experimental Mechanics, Inc. 2013

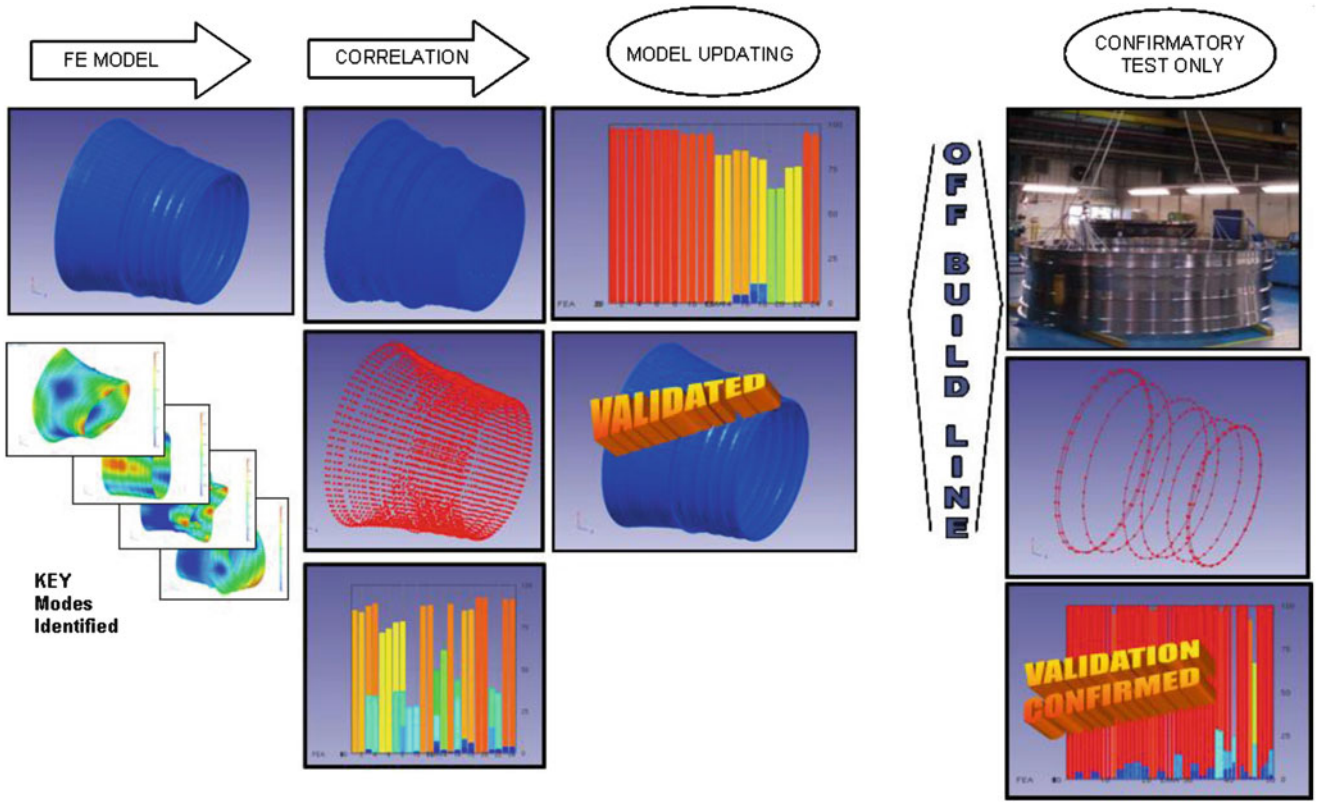

Fig. 2.1 Schematic of a validation of an assembly model

Non-linear testing was initially started with the casing suspended horizontally. It was later decided to rotate the test structure and continue testing with it suspended vertically because some of the natural frequencies obtained from the horizontal tests had shifted slightly.

The assembly has over 50 modes below 1 kHz which makes selection of the most suitable modes for non linear testing difficult.

The testing was divided into five distinct stages

(i) Linear FMFEM model validation
(ii) Mode shape selection
(iii) Qualitative assessment of non linearity using force control method (low excitation levels)
(iv) Quantitative assessment of non linearity of selected resonances using force control method
(v) Higher amplitude modal testing using amplitude control method of those modes identified as non linear.

Using this approach those resonances likely to exhibit the strongest non linear behaviours can be quickly shortlisted. For the assembly the bolted flanges are responsible for most (if not all) of the non linearity of the structure. The testing presented here was focused mainly on excitation of modes with significant casing flange response.

For some engine components, the 'physics' of the undamped FE model are completely represented when analysed in a Free-Free state (i.e. no boundary conditions or external loads applied). In other words, the accuracy of the normal modes prediction of such FE models (i.e. the natural frequencies and mode shapes) are most strongly dependant on the fidelity of the FE model geometry, the material properties used, selection of element type(s) and the degree of FE mesh refinement employed. In fact, for lightly damped, solid, isotropic components at room temperature, the accuracy of the FE model normal modes analysis, for all practical purposes, depends only on these parameters for low levels of excitation.

Early on in the development program, prior to the manufacture of hardware, only nominal geometry models are usually available. Even so, it is clear that if FE models of high geometric fidelity and mesh refinement are generated (i.e. FMFEMs) the resulting predictions of frequencies and mode shapes can be used, well in advance of any Modal Testing, to help validate the less refined and more idealised Whole Engine Models (WEM) required early on in an Engine Development Program. The effort required to produce FMFEMs is now considerably less than might be expected (typically only 2–3 days) depending on the component complexity and the quality of the 3D geometry initially provided. Figure 2.1 shows how a validation of a

linear WEM assembly model can be performed very quickly using FMFEM models where modal testing plays an important part in confirming the quality of the validation process.

At this time it is felt that some limited, confirmatory testing, of the actual component hardware would still be advantageous. This would primarily be to confirm that the test hardware supplied was close to its design intent. It has been shown recently that the use of new technologies such as Scanning LDV systems can be used to rapidly validate FMFEMs. Such short test times can be fitted neatly within modern development engine build programmes with minimal disruption. One of the key advantages of performing modal testing with an SLDV system is its ability to measure mode shapes with high spatial resolution very quickly. Visualization of the mode shapes helped to rapidly identify those resonances which were more likely to exhibit a non-linear response. Reviewing such high fidelity depictions of the assembly mode shapes was very useful for understanding which modes were likely to exercise the casing flanges, the greatest potential source of the assembly non-linearity. This approach was found to be extremely useful for the initial experimental assessment of the casing's likely non linear responses.

2.2 Test Planning for Rapid Validation of FMFEM Axisymmetric Casings and Assemblies

2.2.1 Contrast with WEM Model Validation Testing

For WEM models current validation processes require that all key modes are acquired during the modal test model correlation and to permit any subsequent Computational Model Updating (CMU) required later. When Test Planning for FMFEMs only those key modes need to be acquired which confirm, with high confidence, that the FMFEM closely represents the dynamic behaviour of the test component and so was a valid reference for previous validation of the WEM model.

Modal Test Planning and Validation of WEM models starts with the WEM model itself, however when a FMFEM model has already been used to 'validate' the less detailed WEM model earlier in the engine development programme then a smaller scale modal test can be planned. For example, Test Planning the validation of WEM models will usually make provision to acquire both orthogonal modes from each mode pair. However, when validating large, *strongly* axisymmetric FMFEM models usually only one orthogonal mode from each pair need be acquired on test, since a strong correlation with one of the orthogonal modes would imply a similarly strong correlation for the other. High confidence in the FMFEM also makes it very unlikely that the modal validation test data will need to be used as a reference for any CMU later.

2.2.2 Reducing Modal Test Times

There are three main areas in which to speed up the validation testing required for FMFEMs. This section illustrates some suggestions to reduce the model validation test time required for FMFEM components and/or subassemblies from delivery of the hardware to the test area.

For large casing structures modal test setup times can still be lengthy despite the apparent simplicity of the Free-Free boundary conditions required. However, by using the FMFEM model it becomes possible to predict the test component's fundamental Free-Free mode and mass with high confidence. Using this information the number and stiffness of the suspension points required can be calculated in advance and can be made ready prior to the test hardware's arrival.

Correctly marking up the test hardware prior to modal testing is critical, as it locates the test positions carefully chosen during Test Planning onto the actual test hardware. Mistakes made during marking-up are often difficult to evaluate post test and will artificially reduce the correlation with the FMFEM model.

The large amount of geometric detail in FMFEMs can be utilised to simplify marking-up of the test hardware enormously. A large number of features (e.g. flange holes, casing holes, casing bosses, etc.) within the FMFEM can now also be accurately located on the test hardware itself. Higher initial confidence in the FMFEM also means that fewer test points are required for validation, i.e. additional test points that would otherwise have been specified to extract both orthogonal mode pairs or to aid mode visualisation are no longer required.

It will be shown that for large axisymmetric component casings (and subassemblies) test data will usually only be required from a sector of the test hardware in order to validate its corresponding FMFEM model with high confidence. Since only one side of the component needs to be tested, non-contact 'line of sight' dynamic measurement methods (e.g. SLDV) can

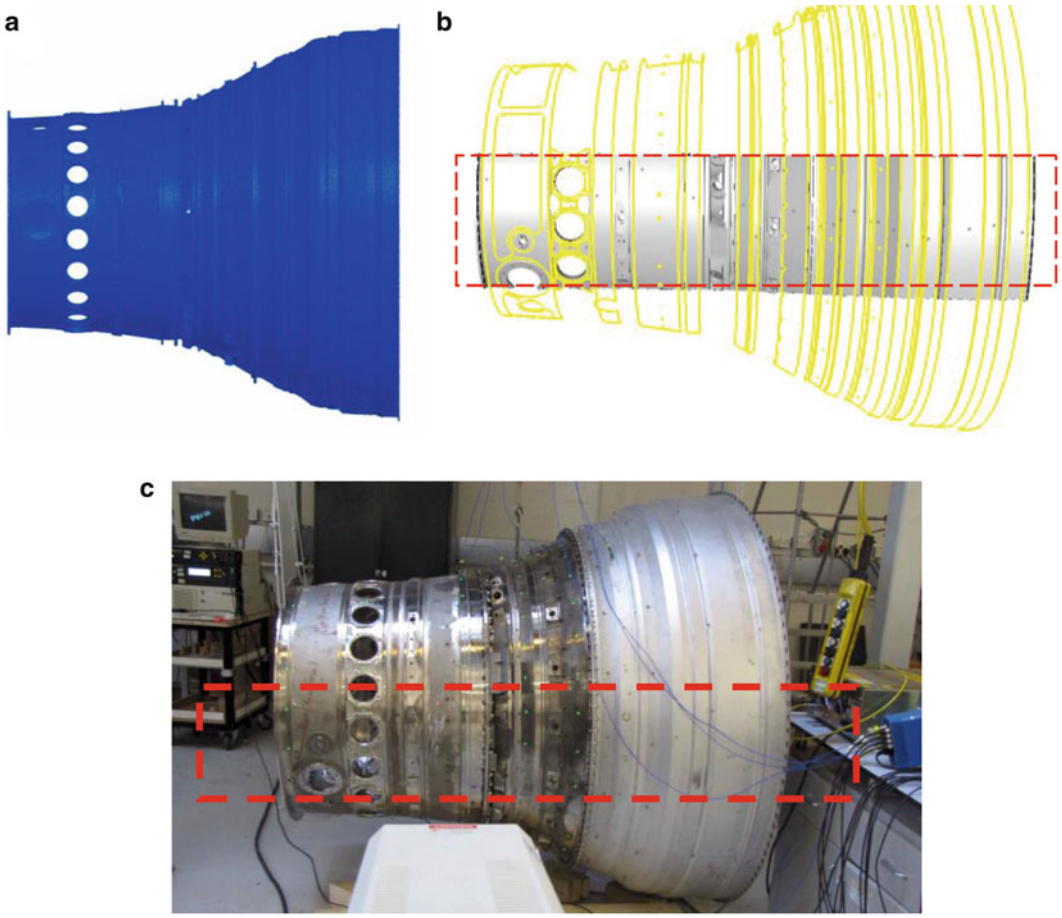

Fig. 2.2 FE model **(a)**, target sector **(b)** and test setup **(c)**. **(a)** Mesh Finite Element Model (FMFEM) of the COC/HPTIPT/LPT casing assembly. **(b)** Target sector used for the Test planning of COC/HPTIPT/LPT casing assembly FMFEM. **(c)** Setup showing the target sector of the FMFEM on the real COC/HPTIPT/LPT casing assembly

be employed efficiently. When SLDV is used the acquisition can also be automated to give high density area scans. It is essential to confirm in advance, using Test Planning, that the chosen sector scan is likely to provide sufficient high quality data in order to validate the target FMFEM modes.

2.2.3 Sector Test Planning for Large Axisymmetric FMFEMs

Figure 2.2a shows a FMFEM model of a large Civil Engine casing sub-assembly. This FMFEM model has over 12 million degrees of freedom and the casing flanges have been modelled (simplistically) as rigidly fixed together. Using the Rolls-Royce in-house FE code it is possible to quickly 'hide' all but a sector of the full assembly model, Fig. 2.2b, and export selected nodal displacements from that sector only. Figure 2.2c shows how closely the geometry of the FMFEM sector matches the actual test hardware; a number of the same features can be clearly identified on both (e.g. casing holes, bosses, etc.). Note, not all sector faces are chosen for inclusion in Test Planning, highly angular faces (e.g. bosses, flange radii, etc.) have not been included and so appear uniformly dark blue (i.e. no displacement data exported) in Fig. 2.2c.

The first 30 FMFEM modes were included in Test Planning. The displacement data and sector FE mesh were combined and converted into a format that could be read directly into FEMtools [2]. Using FEMtools it was possible to quickly produce an autoMAC of the sector displacement patterns from the first 30 FMFEM modes. This was one of the key aims of Test Planning – to eliminate or minimise any spatial aliasing, i.e. to ensure that enough test points are included so that *all modes of interest* could be unambiguously differentiated.

In this way testing a 'sector' of the FMFEM was 'simulated' in order to determine how many test points might be required to clearly differentiate the first 30 modes of the sub-assembly on test. The autoMAC of a good test plan will have

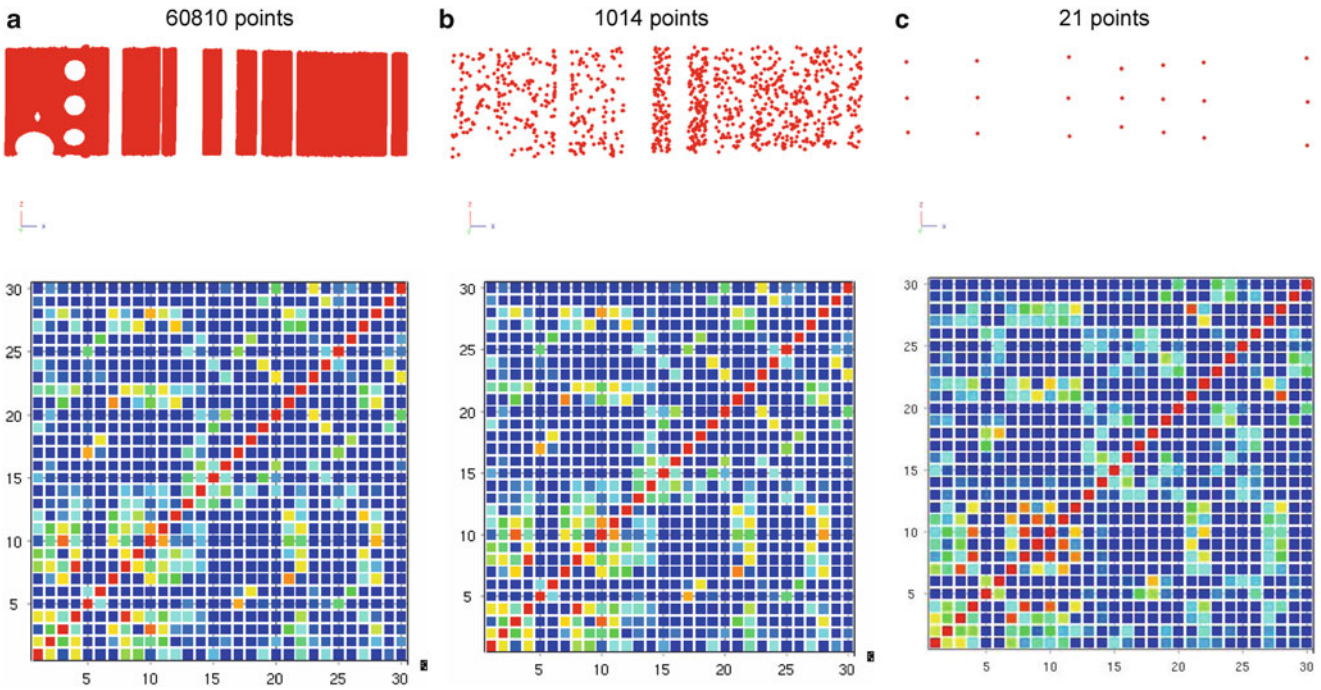

Fig. 2.3 Predicted variation in the autoMAC of first 30 modes of the FMFEM sector due to a reduction in test point density

low off-diagonal terms for all modes of interest. Figure 2.3 shows the effect on the autoMAC for a reducing number of test points assumed from (a) all 60,810 points exported from the FMFEM; to (b) a subset of 1,014 points; to (c) where only 21 points were selected. Assuming 60,810 test points is obviously impractical, however, the resulting autoMAC does provide a useful datum against which to assess how decreasing test point density might adversely affect the resulting test.

It can be seen that a reduction from 60,810 to 1,014 test points, a far more likely scan density for this structure, has had little detrimental effect on the autoMAC. A Test Plan is usually deemed satisfactory if the off diagonal terms of the simulated test autoMAC are less than 40% for all key modes unless they are already well separated (>25%) in frequency. In other words, no two modes on test should look too much alike unless they can also be differentiated (with high confidence) using frequency difference alone. The near identical autoMAC's of Fig. 2.3a, b show that using 1,014 test points would be functionally as good as using 60,810 points.

What may be a little more surprising is that the autoMAC from a very small (but carefully chosen) number of test points, i.e. the 21 points of Fig. 2.3c, is still reasonable. While there are now some obvious differences when compared with the larger tests, its autoMAC suggests that test data from just these 21 points would still lead to a satisfactory modal test.

The number and location of the accelerometers required for the modal test should always be confirmed using Test Simulation. A key advantage for FMFEM validation testing is that it becomes possible, during Test Simulation, to confirm a number of suitable accelerometer positions which also take advantage of the very high geometry fidelity to the actual test hardware. Through careful Test Planning, the number and position of the test accelerometers required can be chosen such that they that are simple to attach accurately, and very quickly, to the test hardware.

2.3 Test Case: SILOET 2.3.2: Full Assembly COC\HPTIPT\LPT FMFEM

In order to demonstrate the applicability of the above approach it was decided to conduct some rapid testing of the large Civil casing sub-assembly shown in of Fig. 2.2a, at the University of Bristol as part of the SILOET Research Program. The Test Planning and Test Simulation outlined in Sect. 2.2.3 were carried out by Rolls-Royce and an impact hammer modal test was conducted at the University of Bristol using just the 21 points of Figs. 2.3c and 2.10 off pre-selected reference accelerometer positions around the assembly. The location of these 21 points on the test hardware has been shown in Fig. 2.4.

The results of the testing are shown in Table 2.1 where it can be seen that there is strong correlation with the FMFEM predictions for at least 1 of each orthogonal mode pair up to mode pair 12. Table 2.1 compares the FMFEM correlation

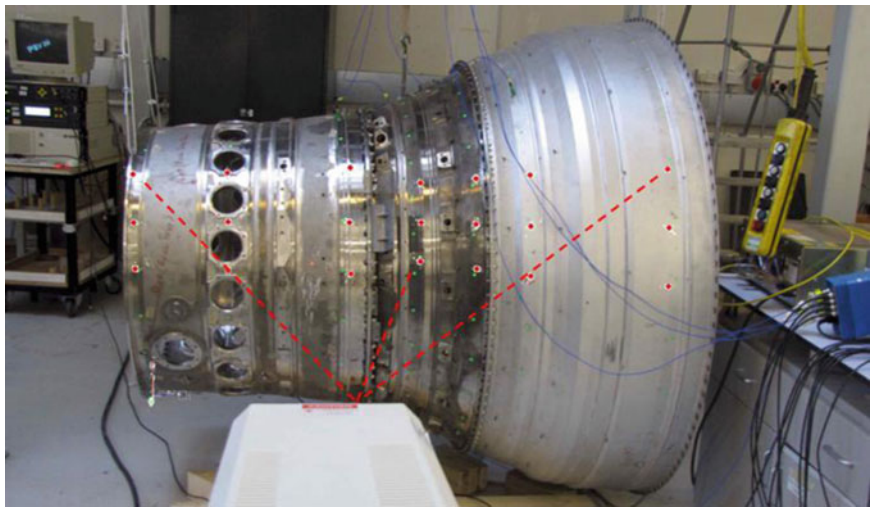

Fig. 2.4 Location of the 21 measurement points

Table 2.1 Correlation of FMFEM model against modal test data. Comparison of rapid sector test FMFEM correlation with that of the full modal test

					Full test		Rapid test	
Mode pair	FMFEM mode	Hz	TEST mode	Hz	Freq. diff. (%)	MAC	Freq. diff. (%)	MAC
1	1	39.3	1	39.1	0.4	97.8	−0.9	91.3
	2	40.1	2	39.7	1.1	94.4	2.5	80.9
2	3	53.7	3	53.1	1.1	99.0	1.1	96.3
	4	53.8	4	53.2	1.2	99.2	1.1	89.1
3	5	58.7	5	58.5	0.3	97.4	−0.4	95.2
	6	58.7	6	58.9	−0.3	97.1	0.4	90
4	7	84.5	7	82.3	2.7	99.5	2.7	97.8
	8	84.6	8	82.4	2.7	99.1	2.7	94.4
5	9	129.3	9	125.7	2.9	98.8	2.8	96.1
	10	129.3	10	125.8	2.8	99.0	2.9	90.6
6	11	185.5	11	180.5	2.8	97.3	2.8	98.5
6	12	185.6	12	180.6	2.8	96.9	2.8	79.3
7	13	201.8	13	187.7	7.5	85.9	7.5	92.2
	14	203.0	14	189.4	7.2	96.3	7.2	95.2
8	15	206.8	15	201.1	2.9	96.9	0.4	97.1
	16	209.9	16	206.0	1.9	97.3	4.4	96.4
9	17	241.2	17	229.8	4.9	92.2	4.9	94.8
	18	242.4	18	230.3	5.3	91.6	5.3	89.5
10	19	244.8	19	232.7	5.2	98.4	5.2	97.3
	20	245.0	20	233.2	5.0	93.1	5.1	90.9
11	21	249.6	21	242.6	2.9	98.9	2.9	96.6
	22	249.7	22	243.0	2.8	99.1	2.8	93.4
12	23	290.1	23	283.5	2.3	99.4	1.9	93.5
	24	290.5	24	284.8	2.0	99.4	2.5	96.2

results of the 21 point sector test and those of the larger 200 point whole annulus test. The 21 point ‘sector’ test and 200 point ‘full’ modal test results compare well in almost all cases, and very well for at least one of the orthogonal modes in each pair – which was the original aim of the Test Planning. For both tests mode pair 7, 9 and 10 are outside the current FMFEM acceptance criteria and this is likely due to the simplistic modelling of the flange joints in the FMFEM (fully fixed) causing it to over predict the frequencies for these modes. The advantage of SLDV scanning is that it can be completely automated and gives very high test point density (typically 1,000+ points). However, it generally uses a ‘contacting’ excitation system (e.g. a small Electromagnetic (EM) shaker) which can have a negative impact on the extraction of the orthogonal mode pairs of the large axisymmetric components/sub-assemblies and also on their measured frequencies (due to mass attachment effects).

2.4 Test Setup for Non-linear Large Assembly Tests

2.4.1 Preliminary Measurements

The initial assessment of the casing assembly's non linearity was started with it suspended horizontally. The ten off reference accelerometer positions used during the linear validation of the assembly were also used for the non linear testing to provide continuity. Figure 2.5 shows the initial non linear test set-up, and the LDS V200 electromagnetic shaker (20 N dynamic range) attached to the HPIPT of the casing.

Although a commercially available system was used for the non-linear testing, a customised acquisition panel was created in LabVIEW (a National Instruments software package) to support the initial investigation. The test data acquired was analysed using the ICATS modal analysis software suite [3].

A broadband sine step excitation (500 Hz bandwidth) was selected to excite a pre-chosen subset of the casing resonances for non linear assessment. Figure 2.6 shows in red boxes the resonances selected at 58, 206, 232 and 460 Hz, respectively. Neither the force nor amplitude was experimentally controlled but instead, as a first pass check, the selected resonances were excited at increasing levels in order to visually detect any changes in the resulting FRFs, that might be suggestive of underlying non linearity.

As a quick first pass check, neither the force nor amplitude was experimentally controlled but instead the selected resonances were excited at increasing levels in order to visually detect any changes in the resulting FRFs, which might be suggestive of underlying non linearity. In order to excite to higher amplitudes a further trial was carried out with a larger shaker LDS V400 which has a 190 N dynamic range.

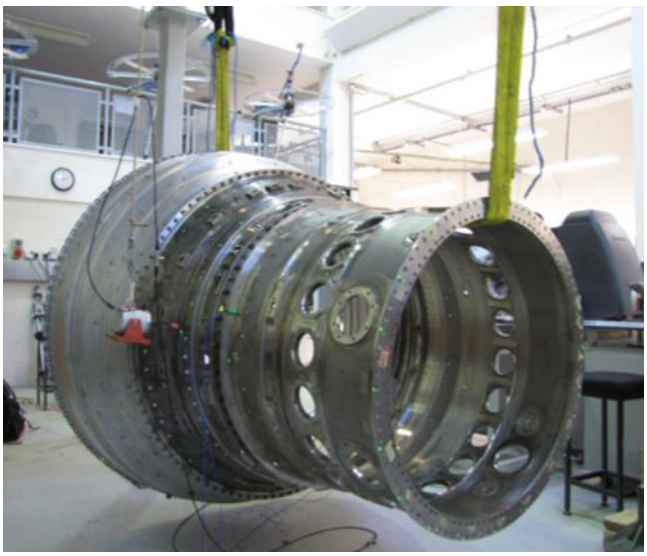

Fig. 2.5 Test rig setup horizontally

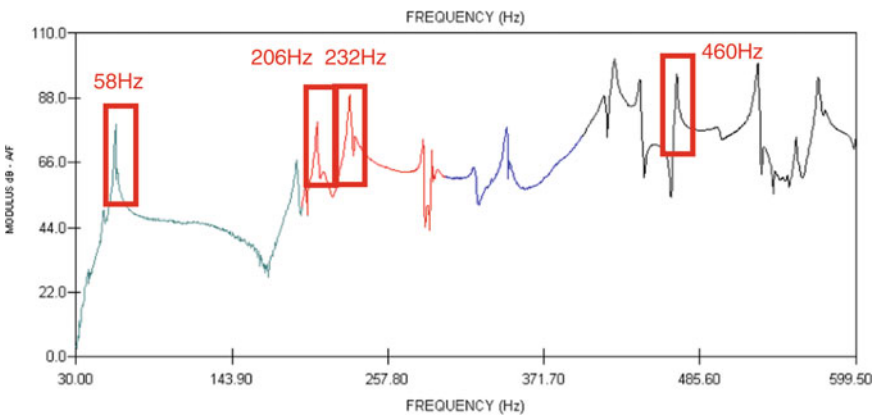

Fig. 2.6 Broad band excitation for resonance's selected